Structural Properties and Control of Soft Robots Modeled as Discrete Cosserat Rods

Lekan Molu and Shaoru Chen

***Abstract*— Soft robot models featuring approximate finite-dimensional reduced-order models (undergoing small deformations) are increasingly becoming paramount in literature and applications. In this paper, we consider the piecewise constant strain (PCS) discrete Cosserat model whose dynamics admit the standard Newton-Euler dynamics for a kinetic model. Contrary to popular convention that soft robots under these modeling assumptions admit similar mechanical characteristics to rigid robots, the schemes employed to arrive at the properties for soft robots under finite deformation show a far dissimilarity to those for rigid robots. We set out to first correct the false premise behind this syllogism: from first principles, we established the structural properties of soft slender robots undergoing finite deformation under a discretized PCS assumption; we then utilized these properties to prove the stability of designed proportional-derivative controllers for manipulating the strain states of a prototypical soft robot under finite deformation. Our newly derived results are illustrated by numerical results on a single arm of the Octopus robot and demonstrates the efficacy of our designed controller based on the derived kinetic properties. This work rectifies previously disseminated kinetic properties of discrete Cosserat-based soft robot models with greater accuracy in proofs and clarity.**

I. Introduction

Soft robots are attracting wide adoption in the automation community owing to their improved bending, torsion, configurability, and compliance properties. These have fostered applications including customizable solutions for assistive wearable devices [23, 1], robot grippers [12], and mobile robots [13] among others. For a soft robot to be useful in the physical world, its body deformation and internal actuators must be strategically well-regulated, often via a careful control system. Such control strategies require a high-fidelity mathematical model of its dynamics. While machine learning (ML) do provide black-box models, in practice these models are non-interpretable, lacking reliability, and failing to account for the delicate and continuous coupled interaction between the soft arm material, its internal actuators, and the external environments' affordances. There is a growing consensus in the soft robotics community that ML models are inefficient for integrating body compliance [14] with embodied intelligence [24] towards soft robots that exploit their functional flexible nature to achieve precise and adept manipulation [14].

A good control strategy for a soft robot is one that matches its complex internal dynamical structure with the physical interactions on the external environment. It has been argued recently [7] that a model-based control design principle is needful to fully realize the compliance and deformation efficacy for soft robots in the physical world [7, 14]. A model-based control scheme would require a good mathematical model of its internal dynamics. Since soft robots exhibit exhibit infinite degrees-of-freedom (DoF) when modeled exactly as a continuum body, (nonlinear) partial differential equations (PDEs) are the standard mathematical modeling tools for analysis – owing to their distributed mass. However, scanty theory exists for nonlinear PDEs analyses and researchers have for the time being exploited the modeling success stories that based on approximate finite-dimensional ordinary differential equations (ODEs) [7].

Tractable reduced-order mathematical models are typically formulated by restricting the range of shapes of the continuum robot to a finite-dimensional functional space over a curve that parameterizes the robot. Essentially, this is equivalent to taking finite nodal points on the soft robot's body and approximating the dynamics along the discrete sections between the nodes by an ODE. An aggregated ODE of all discretized sections can then be used to model the dynamics of the entire discretized continuum robot. A paramount example is the discrete Cosserat model of Renda et al. [18] whereupon the nonlinear PDE that describes the robot's kinetics in exact form is rendered in the form of standard Newton-Euler ODEs via D'Alembert's principle of cvirtual work. This is done by forming piecewise constant strain (PCS) sections on discretized specific nodal points of the continuum soft robot. This PCS mathematical model lends itself well to slender soft robots that can be controlled to arbitrary accuracy depending on the discretization resolution of the constant strain sections. The PCS model is attractive for model-based control since it addresses torsion, in-plane, and out-of-plane (multi-) bending motions with finite ordinary differential equations (ODEs) in the form of the standard Newton-Euler dynamic equations.

In this paper, a strain-parameterized PCS dynamics on a reduced special Euclidean-3 group ($\mathbb{SE}(3)$) is considered for analysis and control. This model outperforms the common piecewise constant curvature (PCC) [22, 17] and the constant curvature variants [9] used outside of finite element modeling methods (FEM) [6]. In this sentiment, we prove the structural properties of Renda et al. [18]'s derived Newton-Euler (N-E) equations. It is noteworthy to emphasize that our work establishes from first principles the structural properties of soft robot kinetic equations that are assumed to be similar to those of rigid robots as in [16] and [5]. We, in fact, establish that the components of the tensors for soft and rigid robots are different and the proofs for the structural

The authors are with Microsoft Research, NYC. Emails: {lekanmolu, shaoruchen}@microsoft.com.

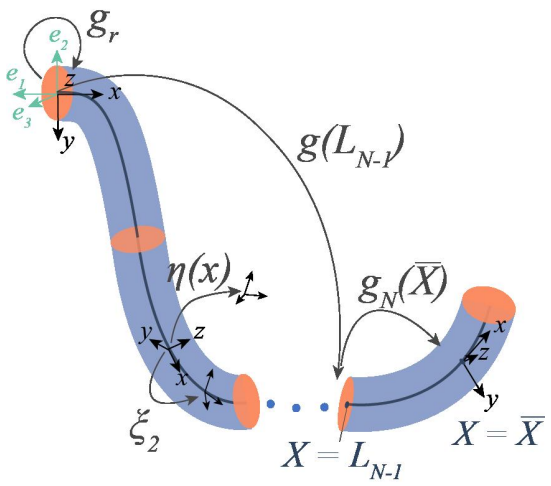

Fig. 1. Schematic of the kinematics of the piecewise constant strain model. See Section II-B for the notations in this figure.

properties of a soft robot follow a different route since being continuum, they exhibit distributed mass densities. Afterwards, we then exploit the geometric properties of the derived N-E dynamics for control tasks. We consider a single arm of the CyberOctopus [20] (configuration shown in Fig. 1) to benchmark our controllers *on the characteristic in-plane bending deformation which is difficult to model with PCC and control*. The choice of the example is motivated by the fact that the Octopus robot [11] blends the interplay between continuum mechanics and sensorimotor control well and offers a numerical simulation framework upon which we can verify our theoretical results.

The rest of this paper is structured as follows: in §II, we introduce notations and provide a non-exhaustive background. The theoretical machinery for the rest of the paper are introduced in §III. A multivariable stabilizing feedback controller for regulating the tip point and strain states is presented in §IV. Section V describe our numerical results and we conclude the paper in §VI.

II. Preliminaries on The PCS Model

We describe the soft arm's (Fig. 1) PCS model in what follows.

A. Microsolid Configuration

The PCS model is derived from the continuous Cosserat model [2] which views the soft robot arm as an ensemble of infinitesimal microsolids. Following Renda et al. [18]'s notation, let $X \in [0, L]$ denote the material abscissa along the robot arm, where L is the robot's length. Let $p(X)$ describe the position vector and $R(X)$ denote the corresponding orientation matrix of a microsolid on the robot arm. Then, the robot's configuration space, parameterized by a curve $g(X) : X \to \mathbb{SE}(3)$, is $g(X) = \begin{pmatrix} R(X) & p(X) \\ 0^\top & 1 \end{pmatrix}$. Suppose that the strain field and twist vectors are respectively $\eta \in \mathbb{R}^6$ and $\xi \in \mathbb{R}^6$. The arm's strain field is a state vector along the curve $g(X)$ defined as $\breve{\eta}(X) = g^{-1}\partial g/\partial X$, and the velocity of $g(X)$ is the twist vector field $\breve{\xi}(X)$ defined as $\breve{\xi}(X) = g^{-1}\partial g/\partial t$. We denote $\breve{\eta}$ ($\breve{\xi}$) as the isomorphism from η (ξ) $\in \mathbb{R}^6$ to its matrix representation in $\mathfrak{se}(3)$, i.e., the Lie algebra of $\mathbb{SE}(3)$.

In what follows, for a configuration $\boldsymbol{g}(X) \in \mathbb{SE}(3)$, its adjoint and coadjoint representations are parameterized by the material abscissa and denoted as $\mathrm{Ad}_{\boldsymbol{g}}(X)$ and $\mathrm{Ad}^\star_{\boldsymbol{g}}(X)$, respectively. The corresponding adjoint and coadjoint representation of the strain twist vector are $\mathrm{ad}_{\eta,\xi}(X)$ and $\mathrm{ad}^\star_{\eta,\xi}(X)$, respectively.

As shown in Fig. 1, the transformation from the base to the inertial frame is

$$\boldsymbol{g}_r = \begin{pmatrix} 0 & -1 & 0 & 0 \\ 1 & 0 & 0 & 0 \\ 0 & 0 & 1 & 0 \\ 0 & 0 & 0 & 1 \end{pmatrix}. \tag{1}$$

The continuous Cosserat model is however computationally intensive to employ in practical applications since it requires modeling every particle on the body of the robot and employs partial differential equations to develop a static and dynamic model. Suppose that the deformation under consideration is finite, one can make finite approximations of the strain deformation along segments of the robot between discretized spatial nodal points. Doing this, one obtains a strain dynamics that is composed of the respective piecewise strains of the individual segments of the robot. Discretizing the strain on the robot's body this way by assuming constant strains along sections constitutes the popular piecewise constant strain model [18]. We introduce the PCS model in what follows.

B. Piecewise Constant Strain Model

As shown in Fig. 1, the PCS model divides the soft robot arm into N sections $\{\mathcal{M}_n\}_{n=1}^N$ and assumes that the respective strain η_n is constant for each section. The material abscissa $X \in [0, L]$ is divided into N intervals $[0, L_1], [L_1, L_2], \cdots, [L_{N-1}, L_N]$ with $L_N = L$, and the i-th section $\mathcal{M}_n$ spans $[L_{n-1}, L_n]$. In generalized coordinates, the joint vector of the soft robot is denoted $q(\eta) = [\eta_1^\top, \ldots, \eta_N^\top]^\top \in \mathbb{R}^{6N}$.

Remark 1 (Notations in Fig. 1)**.** *The inertial frame is signified by the basis triad $(\boldsymbol{e}_1, \boldsymbol{e}_2, \boldsymbol{e}_3)$ and $\boldsymbol{g}_r(X)$ is the transformation from the inertial to the manipulator's base frame. For cable-driven arms, the point at which actuation occurs is labeled $\bar{X}$. The configuration matrix that parameterizes curve X of length L_n is denoted $\boldsymbol{g}_{L_n}$. The cable runs through the z-axis in the (micro) body frame (x-axis in the spatial frame).*

The piecewise constant strain assumption greatly simplifies the representation of the kinematics and dynamics of the soft robot. Importantly, it allows the following kinematics relation, $\xi(X) = J(X)\dot{q}$ where the geometric Jacobian $J(X) \in \mathbb{R}^{6\times 6N}$ is given by [18, Eq. (20)] (omitted here due to space limitation) and can be directly calculated from the strains η_n. Using d'Alembert's principle, the generalized dynamics for the PCS model under external and actuation

loads admits the weak form [18]:

$$\underbrace{\left[\int_0^{L_N} J^T \mathcal{M}_a J dX\right]}_{M(q)} \ddot{q} + \underbrace{\left[\int_0^{L_N} J^T \mathrm{ad}^{\star}_{J\dot{q}} \mathcal{M}_a J dX\right]}_{C_1(q,\dot{q})} \dot{q} + \underbrace{\left[\int_0^{L_N} J^T \mathcal{M}_a \dot{J} dX\right]}_{C_2(q,\dot{q})} \dot{q} + \underbrace{\left[\int_0^{L_N} J^T \mathcal{D} J \|J\dot{q}\|_p dX\right]}_{D(q,\dot{q})} \dot{q} - \underbrace{(1-\rho_f/\rho)\left[\int_0^{L_N} J^T \mathcal{M} \mathrm{Ad}^{-1}_{\boldsymbol{g}} dX\right]}_{N(q)} \mathrm{Ad}^{-1}_{\boldsymbol{g}_r} \mathcal{G} - \underbrace{J(\bar{X})^T \mathcal{F}_p}_{F(q)} - \underbrace{\int_0^{L_N} J^T \left[\nabla_x \mathcal{F}_i - \nabla_x \mathcal{F}_a + \mathrm{ad}^{\star}_{\xi_n}(\mathcal{F}_i - \mathcal{F}_a)\right] dX}_{\tau(q)} = 0, \tag{2}$$

where $\mathcal{F}_i(X)$ is the wrench of internal forces, $\mathcal{F}_a(X)$ is the *distributed* wrench of actuation loads, and $\mathcal{F}_e(X)$ is the external *distributed* wrench of the applied forces. The screw mass inertia matrix $\mathcal{M}(X) = \mathrm{diag}(I_x, I_y, I_z, A, A, A)\,\rho$ for a body density ρ, sectional area A, bending, torsion, and second inertia operator I_x, I_y, I_z respectively. In (2), $\mathcal{M}_a = \mathcal{M} + \mathcal{M}_f$ is a lumped sum of the microsolid mass inertia operator, $\mathcal{M}$, and that of the added mass fluid, $\mathcal{M}_f$; $\mathcal{D}(X)$ is the drag matrix; $\|\cdot\|_p$ is the translation norm of the expression contained therein; ρ_f is the density of the fluid in which the material moves; ρ is the body density; $\mathcal{G} = [0, 0, 0, -9.81, 0, 0]^T$ is the gravitational vector; and $\mathcal{F}_p$ is the applied wrench at $\bar{X}$. Using the terms defined by the underbraces in (2), we can rewrite the PCS dynamics in the standard Newton-Euler form as:

$$\begin{aligned} M(q)\ddot{q} + [C_1(q,\dot{q}) + C_2(q,\dot{q})]\,\dot{q} &= \tau(q) + F(q) \\ &\quad + N(q)\mathrm{Ad}^{-1}_{\boldsymbol{g}_r}\mathcal{G} - D(q,\dot{q})\dot{q}, \end{aligned} \tag{3}$$

which has the structure of the Lagrangian model of rigid serial manipulators. In the next section, we prove that the PCS model dynamics (3) of soft robot arms, in addition to its resemblance to the Lagrangian dynamics, also enjoys the basic structural properties of Lagrangian dynamics.

III. Structural Properties of the PCS Model

We now establish the Lagrangian properties of the PCS model dynamics (3).

Theorem 1 (Structural properties of the kinetic equation)**.** *Equation* (3) *satisfies the following properties:*

Property 1 (Positive definiteness of the Inertia Operator)**.** *The inertia tensor $\mathcal{M}_a(q)$ is symmetric and positive definite. As a result $M(q)$ is symmetric and positive definite.*

Proof: [Proof of Property 1] The jacobian, J, is injective by [18, equation 20]. Thus, property 1 follows from its definition.

Property 2 (Boundedness of the Mass Matrix)**.** *The mass inertial matrix $M(q)$ is uniformly bounded from below by $m\boldsymbol{I}$ where m is a positive constant and $\boldsymbol{I}$ is the identity matrix.*

Proof: [Proof of Property 2] This is a restatement of the lower boundedness of $M(q)$ for fully actuated n-degrees of freedom manipulators [19].

Remark 2. *Both properties 1 and 2 are important when deriving feedback control laws that exploit the manipulator's inertial dynamics. Note that results which exist in literature make a naive assumption about the positive-definiteness of $M(q)$, often drawing similarity to those of rigid manipulators. However, rigid manipulators do not have distributed mass matrices as a discretized soft robot has (see* (3)*).*

Property 3 (Skew symmetric property)**.** *The matrix $\dot{M}(q) - 2\left[C_1(q,\dot{q}) + C_2(q,\dot{q})\right]$ is skew-symmetric.*

Proof: [Proof of Property 3] By Leibniz's rule, we have

$$\begin{aligned} \dot{M}(q) &= \frac{d}{dt}\left(\int_0^{L_N} J^T \mathcal{M}_a J dX\right) = \int_0^{L_N} \frac{\partial}{\partial t}\left(J^T \mathcal{M}_a J\right) dX \\ &\triangleq \int_0^{L_N} \left(\dot{J}^T \mathcal{M}_a J + J^T \dot{\mathcal{M}}_a J + J^T \mathcal{M}_a \dot{J}\right) dX. \end{aligned} \tag{4}$$

Therefore, $\dot{M}(q) - 2\left[C_1(q,\dot{q}) + C_2(q,\dot{q})\right]$ becomes

$$\begin{aligned} &\int_0^{L_N} \left(\dot{J}^\top \mathcal{M}_a J + J^\top \dot{\mathcal{M}}_a J + J^\top \mathcal{M}_a \dot{J}\right) dX \\ &- 2\int_0^{L_N} \left(J^\top ad^{\star}_{J\dot{q}} \mathcal{M}_a J + J^\top \mathcal{M}_a \dot{J}\right) dX \qquad (5) \\ &\triangleq \int_0^{L_N} \left(\dot{J}^\top \mathcal{M}_a J + J^\top \dot{\mathcal{M}}_a J - J^\top \mathcal{M}_a \dot{J}\right) dX \\ &\quad - 2\int_0^{L_N} J^\top ad^{\star}_{J\dot{q}} \mathcal{M}_a J dX. \qquad (6) \end{aligned}$$

Similarly, $-\left[\dot{M}(q) - 2\left[C_1(q,\dot{q}) + C_2(q,\dot{q})\right]\right]^\top$ expands as

$$\begin{aligned} &-\dot{M}^\top(q) + 2\left[C_1^\top(q,\dot{q}) + C_2^\top(q,\dot{q})\right] = \\ &\int_0^{L_N} dX^\top \left(-J^\top \mathcal{M}_a \dot{J} - J^\top \dot{\mathcal{M}}_a J - \dot{J}^\top \mathcal{M}_a J\right) \\ &\quad + 2\int_0^{L_N} dX^\top \left(J^\top \mathcal{M}_a ad_{J\dot{q}} J + \dot{J}^\top \mathcal{M}_a J\right) \\ &\triangleq \int_0^{L_N} \left(J^\top \mathcal{M}_a \dot{J} - \dot{J}^\top \mathcal{M}_a J - J^\top \dot{\mathcal{M}}_a J\right) dX \\ &\quad - 2\int_0^{L_N} J^\top ad^{\star}_{J\dot{q}} \mathcal{M}_a J dX \qquad (7) \end{aligned}$$

where the terms in equation (7) *follow from the symmetry of the matrices that constitute the integrands. Inspecting* (6) *and* (7)*, it is easy to see that their right hand sides verify*

the identity

$$\int_0^{L_N}\left(\dot{J}^\top\mathcal{M}_aJ+J^\top\dot{\mathcal{M}}_aJ-J^\top\mathcal{M}_a\dot{J}\right)dX - 2\int_0^{L_N}J^\top ad^\star_{J\dot{q}}\mathcal{M}_aJdX=2\int_0^{L_N}J^\top ad^\star_{J\dot{q}}\mathcal{M}_aJdX- \int_0^{L_N}\left(J^\top\mathcal{M}_a\dot{J}-\dot{J}^\top\mathcal{M}_aJ-J^\top\dot{\mathcal{M}}_aJ\right)dX \tag{8}$$

or

$$\dot{M}(q)-2\left[C_1(q,\dot{q})+C_2(q,\dot{q})\right]= -\left[\dot{M}(q)-2\left[C_1(q,\dot{q})+C_2(q,\dot{q})\right]\right]^\top. \tag{9}$$

A fortiori, the skew symmetric property follows.

Remark 3. *Since $\dot{M}(q)$ is symmetric (cref.* (4)*), another way of stating the skew-symmetric property is to write*

$$\dot{M}(q)=C_1(q,\dot{q})+C_2(q,\dot{q})+\left[C_1(q,\dot{q})+C_2(q,\dot{q})\right]^\top. \tag{10}$$

Owing to the symmetry of the right-hand-side (rhs), we have $\dot{M}=2(C_1+C_2)$.

This skew-symmetric property is a form of the conservation of energy law for a soft robot that can be exploited when deriving Lyapunov-based control laws that achieves asymptotic stability of all system states.

Property 4 (Linearity-in-the-parameters)**.** *There exists a constant vector $\Theta\in\mathbb{R}^l$ and an $N\times l$ dimensional regressor function $Y(q,\dot{q},\ddot{q})\in\mathbb{R}^{N\times l}$ such that*

$$M(q)\ddot{q}+\left[C_1(q,\dot{q})+C_2(q,\dot{q})+D(q,\dot{q})\right]\dot{q}-F(q) - N(q)Ad^{-1}_{\boldsymbol{g}_r}\mathcal{G}=Y(q,\dot{q},\ddot{q})\Theta. \tag{11}$$

Proof: [Proof of Property 4] Consider the generalized constitutive law for the full Cosserat model derived in [3, §6.3]. The reduced Lagrangian density in $\mathfrak{se}(3)$ per unit of deformed volume (for all configurations)[1] *for a configuration $\mathcal{B}$ is $\mathfrak{L}=\mathfrak{T}-\mathfrak{U}$ [3] where $\mathfrak{T},\mathfrak{U}$ respectively denote the volume's left-reduced kinetic and elastic potential energy densities in $\mathcal{B}$. From the Euler-Lagrange equation, we have*

$$\tau_n=\frac{d}{dt}\frac{\partial\mathfrak{T}}{\partial\dot{\eta}_n}-\frac{\partial\mathfrak{T}}{\partial\eta_n}+\frac{\partial\mathfrak{U}}{\partial\xi_n},\quad n=1,\dots,N. \tag{12}$$

Suppose that the material mid-surface crosses the microstructures $\mathcal{M}_i$ which correspond to the mass center, then the kinetic energy density per unit of deformed area and its rate of change w.r.t η are [3]

$$\mathfrak{T}(\eta)=\frac{1}{2}\left\langle\begin{pmatrix}\omega\\ \nu,\end{pmatrix},\begin{pmatrix}\bar{I}\omega\\ \bar{\rho}\nu\end{pmatrix}\right\rangle \tag{13}$$

$$\mathfrak{T}(\dot{\eta})=\frac{1}{2}\left\langle\begin{pmatrix}\dot{\omega}\\ \dot{\nu},\end{pmatrix},\begin{pmatrix}\bar{I}\dot{\omega}\\ \bar{\rho}\dot{\nu}\end{pmatrix}\right\rangle \tag{14}$$

[1]Note that the full Lagrangian density of the soft multisection manipulator is $L_m=\int_0^L\mathfrak{L}(\boldsymbol{g},\xi,\eta)dX$.

where $\bar{\rho}$ and $\bar{I}$ respectively denote the mass and angular inertia density per unit volume. It follows that

$$\partial_\eta\mathfrak{T}=\begin{pmatrix}\bar{I}\omega\\ \bar{\rho}\nu\end{pmatrix},\quad \partial_{\dot{\eta}}\mathfrak{T}=\begin{pmatrix}\bar{I}\dot{\omega}\\ \bar{\rho}\dot{\nu}\end{pmatrix}. \tag{15}$$

In a similar vein, the left invariant density of internal energy $\mathfrak{U}$ is [4]

$$\mathfrak{U}(\xi)=\langle\mathcal{F}_{int},(\xi-\xi^d)\rangle \tag{16}$$

for a desired ξ^d and field of internal force constraints $\mathcal{F}_{int}:X\in[0,L]\to\mathcal{F}_{int}(X)\in\mathfrak{se}(3)$. The potential energy per unit of metric area of the deformed surface (assuming that it is concentrated in the mid-surface) is [3]

$$\partial_\xi\mathfrak{U}=\begin{pmatrix}\partial\mathfrak{U}/\partial\gamma\\ \partial\mathfrak{U}/\partial\varepsilon\end{pmatrix}-\begin{pmatrix}0\\ \varepsilon\end{pmatrix}\mathfrak{L} \tag{17}$$

so that the Euler-Lagrange equation (12) *becomes*

$$\begin{pmatrix}\bar{I}\ddot{\omega}+\dot{\bar{I}}\dot{\omega}\\ \bar{\rho}\ddot{\nu}+\dot{\bar{\rho}}\dot{\nu}\end{pmatrix}-\begin{pmatrix}\bar{I}\omega\\ \bar{\rho}\nu\end{pmatrix}+\begin{pmatrix}\partial\mathfrak{U}/\partial\gamma\\ \partial\mathfrak{U}/\partial\varepsilon\end{pmatrix}-\begin{pmatrix}0\\ \varepsilon\end{pmatrix}\mathfrak{L}. \tag{18}$$

Observe*: Under the PCS assumption, each microsolid is fixed so that the energy density per unit section of metric volume is akin to that of a rigid body. The kinetic and potential energies for the PCS model per section i of N sections becomes*

$$\mathfrak{T}=\frac{1}{2}\sum_{i=1}^{N}\left\langle\begin{pmatrix}{}^{i+1}\omega_i\\ {}^{i+1}\nu_i,\end{pmatrix},\begin{pmatrix}{}^{i+1}\bar{I}_i\ {}^{i+1}\omega_i\\ {}^{i+1}\bar{\rho}_i\ {}^{i+1}\nu_i\end{pmatrix}\right\rangle \tag{19}$$

where ${}^{i+1}\omega_i$ is the angular velocity of section $i+1$ in the frame of section i, ${}^{i+1}\nu_i$ is the linear velocity of section $i+1$ in the frame of section i e.t.c. Similarly, the sectional potential energies are

$$\mathfrak{U}(\xi_i)=\sum_{i=1}^{N}\langle\{\mathcal{F}_{int}\}_i,(\xi_i-\xi_i^d)\rangle. \tag{20}$$

Thus, the kinetic and potential energy are each linear in configuration parameters so that

$$\mathfrak{T}=\sum_{i=1}^{N}\frac{\partial\mathfrak{T}}{\partial\Sigma_i}\Sigma_i=\sum_{i=1}^{N}\Gamma\mathfrak{T}_i\Sigma_i,\qquad \mathfrak{U}=\sum_{i=1}^{N}\frac{\partial\mathfrak{U}}{\partial\Sigma_i}\Sigma_i=\sum_{i=1}^{N}\Gamma\mathfrak{U}_i\Sigma_i \tag{21}$$

where Σ_i is an inertial parameter, $\Gamma\mathfrak{T}_i$ is a function of $q,\dot{q}$ and $\Gamma\mathfrak{U}_i$ is a function of q. Using (21) *and plugging* (15) *and* (17) *into* (12)*, we conclude that the sectionalized piecewise Cosserat dynamics is also linear-in-the-inertial-parameters, given as $\tau(q)=Y(q,\dot{q},\ddot{q})\Theta$, where $Y(q,\dot{q},\ddot{q})$ is the matrix function of $q,\dot{q},\ddot{q}$ and Θ is the matrix of parameters.*

Remark 4. *More often than not, the parameters that constitute the mass intertia matrix and Coriolis forces may be unknown. In such situations, it is desirable to identify these parameters in a data-driven manner. This property states that although the soft manipulator's dynamics is naturally described by a nonlinear PDE, if the robot is discretized into*

piecewise constant strain sections, then its dynamics become linear-in-the-parameters. And standard regression techniques can be applied to identify these parameters (e.g. see [21]).

IV. Multivariable Control

Utilizing the Lagrangian properties established in § III, we now propose a globally asymptotically stabilizing proportional-derivative (PD) controller for the soft robot arm. We show that regarding the generalized torque $\tau(q)$ as a control input, $u(q,\dot{q})$, feedback laws are sufficient for attaining a desired joint configuration.

Theorem 2 (Cable-driven Actuation)**.** *For positive definite diagonal matrix gains K_D and K_p, without gravity/buoyancy compensation, the control law*

$$u(q,\dot{q}) = -K_p\tilde{q} - K_D\dot{q} - F(q) \tag{22}$$

under a cable-driven actuation globally asymptotically stabilizes system (3)*, where $\tilde{q}(t) = q(t) - q^d$ is the joint error vector for a desired equilibrium point q^d.*

Proof: Without gravity, the term $N(q)\mathrm{Ad}_{g_r}^{-1}\mathcal{G} = 0$. Let

$$\breve{C}(q,\dot{q}) = C_1(q,\dot{q}) + C_2(q,\dot{q})$$

and write (3) for an arbitrary control input $u(q)$ as

$$M(q)\ddot{q} = u(q,\dot{q}) + F(q) - \left[\breve{C}(q,\dot{q}) + D(q,\dot{q})\right]\dot{q}. \tag{23}$$

Consider the Lyapunov candidate function

$$V(q) = \frac{1}{2}\dot{q}^\top M(q)\dot{q} + \frac{1}{2}\tilde{q}^\top K_p\tilde{q}. \tag{24}$$

Observe: $V(q) > 0, \forall q \neq q^d, \dot{q} \neq 0$, and $V(q) = 0$ when $q = q^d$, $\dot{q} = 0$ in the joint space. Differentiating $V(q)$ yields

$$\begin{aligned}
\dot{V}(q) &= \dot{q}^\top M(q)\ddot{q} + \frac{1}{2}\dot{q}^\top\dot{M}(q)\dot{q} + \tilde{q}^\top K_p\dot{\tilde{q}},\\
&= \dot{q}^\top\left(u(q,\dot{q}) + F(q) - \left[\breve{C}(q,\dot{q}) + D(q,\dot{q})\right]\dot{q}\right)\\
&\quad + \frac{1}{2}\dot{q}^\top\dot{M}(q)\dot{q} + \tilde{q}^\top K_p\dot{q},\\
&= \dot{q}^\top\left(u(q,\dot{q}) + F(q) - \left[\breve{C}(q,\dot{q}) + D(q,\dot{q})\right]\dot{q}\right)\\
&\quad + \tilde{q}^\top K_p\dot{q} + \dot{q}^\top\left[\frac{1}{2}\left(\dot{M}(q) - 2\breve{C}(q,\dot{q})\right) + \breve{C}(q,\dot{q})\right]\dot{q},\\
&= \dot{q}^\top\left[u(q,\dot{q}) + F(q) + K_p\tilde{q} - D(q,\dot{q})\dot{q}\right]
\end{aligned} \tag{25}$$

where the last line follows from the skew symmetric property established in Remark 3. With the control law (22), we have

$$\dot{V}(q) = -\dot{q}^\top\left[K_D + D(q,\dot{q})\right]\dot{q} \leq 0 \tag{26}$$

since K_D is a positive diagonal matrix and the drag term $D(q,\dot{q}) > 0$. Thus, we have that $V(q)$ is decreasing if $\dot{q}$ is non-zero. From (26), it is possible that $\dot{q} = 0$ when $q \neq q^d$. To prove global asymptotic stability, suppose the domain $q \in \Omega \subset \mathbb{R}^{6N}$ is the compact, positively invariant domain with respect to (3). Let $\mathcal{E}$ be the set of all $q \in \Omega$ where $\dot{V}$ is identically zero. Then, for any $q \in \mathcal{E}$, (26) implies that $\dot{q} = 0$ and $\ddot{q} = 0$. From (23), we must have

$$M(q)\ddot{q} + \left[\breve{C}(q,\dot{q}) + D(q,\dot{q})\right]\dot{q} = -K_p\tilde{q} - K_D\dot{q} \tag{27}$$

which implies that $0 = -K_p\tilde{q}$ and hence $q = q^d$. If Υ is the largest invariant set of $\mathcal{E}$, then by LaSalle's invariance theorem [10], every solution starting in Ω approaches Υ as $t \to \infty$. Whence, the equilibrium q^d is globally asymptotically stable.

Corollary 1 (Fluid-driven actuation)**.** *If the robot is operated without cables, and is driven with a dense medium such as pressurized air or water, then the term $F(q) = 0$ so that the control law $u(q,\dot{q}) = -K_p\tilde{q} - K_D\dot{q}$ globally asymptotically stabilizes the system.*

V. Numerical Results

Our goal is to regulate the strain and strain velocity states of the robot per section under different constant tip loads *despite the inevitable non-constant loads due to gravity, external forces, and inertial forces*.

A. System Setup and Parameters

As seen in Fig. 1, the tip load acts on the $+y$-axis in the robot's base frame. We use $\mathcal{F}_p^y$ to represent the tip load acting along the $+y$ direction in what follows. We assume a (near-incompressible) rubber material makes up the robot's body and set its Poisson ratio to 0.45. The mass is chosen as $\mathcal{M} = \rho[I_x, I_y, I_z, A, A, A]$ for a cylindrical soft shell's nominal density of $\rho = 2,000kgm^{-3}$ as used in [18]. We set the cross-sectional area as $A = \pi r^2$ so that $I_x = \pi r^4/2$. The drag screw stiffness matrix D in (3) is a function of each section's geometry and hydrodynamics so that $D = -\rho_w\nu^T\nu\breve{D}\nu/|\nu|$ where ρ_w is the water density set to $997kg/m^3$, and $\breve{D}$ is the tensor that models the geometry and hydrodynamics factors in the viscosity model (see [18, §II.B, eq. 6]). The curvilinear abscissa, $X \in [0, L]$ was discretized into 41 microsolids per section.

B. Discussion

We adopt the recursive articulated-body algorithm [8] and integrate the right-hand-side of the differential equation (23) using a Runge-Kutta-Fehlberg (RKF) adaptive scheme implemented in Python and Torch [15] with relative and absolute errors respectively set to 10^{-7} and 10^{-9}. We found these tolerance values to be crucial for a successful numerical integration scheme as it avoids numerical instability. Depicted on the vertical axes of each chart of Fig. 2 are the strain positions or twists along $+y$-direction (on the robot's local frame) while the horizontal axes depict the number of adaptive RKF (re-) integration steps per for every tenth of a second. The trajectory evolution over time per discretized Cosserat section is shown in the various "dash-dotted" lines, while the "solid blue" lines denote the reference. The controller parameters are annotated within the chart together with the amount of constant tip load in Newtons. We see that all joint configurations are stabilized to reference strain twist states ($\dot{q}^d$) for respective constant tip loads. It can also be inferred that more sections in the discretized Cosserat model lead to less bumpy state regulation.

In (*a1–a3*), the strain twists are precisely regulated to zero offset errors despite large constant tip loads (*a1-a3*); and

a1) Cable-driven, strain twist setpoint terrestrial control.

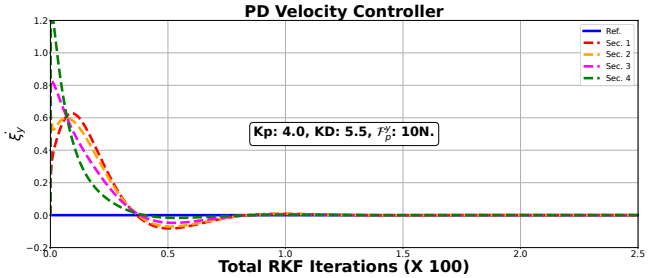

a2) Fluid-actuated, strain twist setpoint terrestrial control.

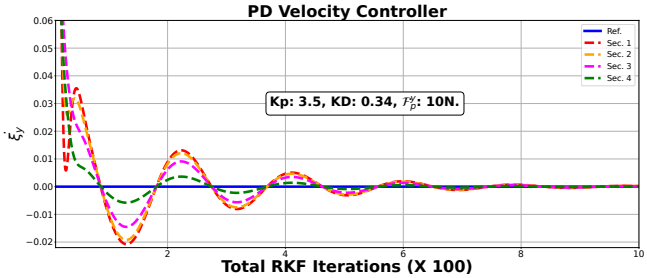

a3) Fluid-actuated, strain twist setpoint underwater control.

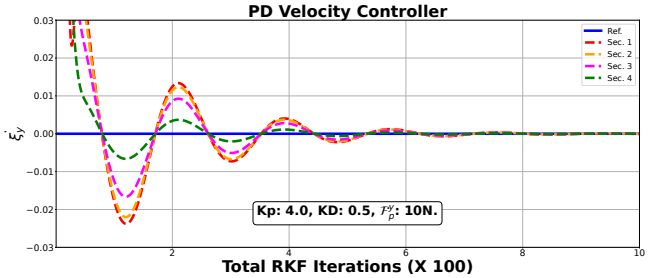

a4) Cable-driven, strain twist setpoint regulation.

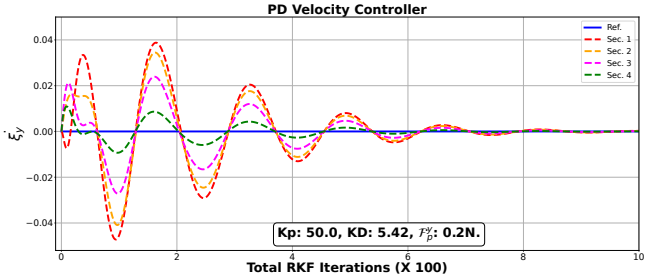

a5) Cable-based position control with a small tip load, 0.2N.

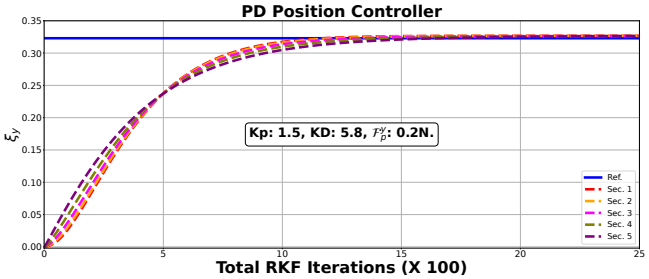

a6) Terrestrial position control.

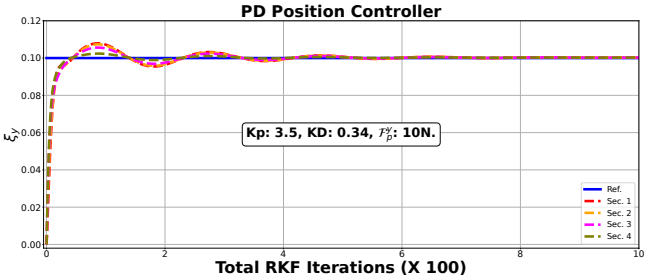

Fig. 2. *(a1 – a3):* Linear strain twist state regulation for a 4-section (41 microsolid pieces per section) soft arm under a $10N$ lateral tip load, $\mathcal{F}_p^y$ that is *(a1)* cable-driven in a sparse medium *(a2)* fluid-actuated in a sparse medium. *(a3)* fluid-actuated in a dense medium such as water (i.e. with drag forces compensation). *(a4)* Under a miniature tip-load of $0.2N$, a cable-driven 4-section arm finely regulates strain twists to equilibrium over time. *(a5)*: Linear strain position regulation for a cable-driven arm operating in air and **(a6)** a fluid-actuated arm illustrating the effect of steady state errors. The horizontal axes show the number of (re)-integration time-steps per second for the adaptive Runge-Kutta-Fehlberg integrator we utilized in computing the controllers.

with small tip disturbances *(a4)*. Notably, the large value of the proportional gain causes overdamping in the transients before convergence. In **(a5)**, with a small tip load of $0.2N$, we notice a critically damped system response. For a fixed setpoint, a reasonable proportional gain $(3.5-4.0)$, followed by a small derivative gain $(0.3-0.5)$ is sufficient to regulate all linear position and velocity states to equilibrium as seen in the **(a6)** chart of Fig. 2.

VI. Conclusion

We have presented the Lagrangian properties for soft robots under a discrete Cosserat model. These properties were then exploited to cancel out nonlinearities in the derived controllers for strain states regulation. Our numerical experiments confirm the conclusions from our Lyapunov analyses. Similar to rigid robots under PD control laws with Lagrangian dynamics, we have observed strain position steady state offsets. Position control efficacy are shown to improve if gravity and/or buoyancy is compensated in the control law.

VII. Acknowledgment

A rising vote of thanks to James Forbes and Audrey Sedal of McGill University's Mechanical Engineering department for early manuscript feedback.

References

[1] Gunjan Agarwal, Nicolas Besuchet, Basile Audergon, and Jamie Paik. Stretchable Materials for Robust Soft Actuators Towards Assistive Wearable Devices. *Scientific reports*, 6(1):34224, 2016.

[2] Stuart S Antman. Problems in nonlinear elasticity. *Nonlinear Problems of Elasticity*, pages 513–584, 2005.

[3] Frederic Boyer and Federico Renda. Poincaré's Equations for Cosserat Media: Application to Shells. *Journal of Nonlinear Science*, 27(1):1–44, 2017. ISSN 14321467.

[4] Frederic Boyer, Mathieu Porez, and Alban Leroyer. Poincaré–cosserat equations for the lighthill three-dimensional large amplitude elongated body theory: application to robotics. *Journal of Nonlinear Science*, 20:47–79, 2010.

[5] Brandon Caasenbrood, Alexander Pogromsky, and Henk Nijmeijer. Energy-shaping controllers for soft robot manipulators through port-hamiltonian cosserat models. *SN Computer Science*, 3(6):494, 2022.

[6] Eulalie Coevoet, Adrien Escande, and Christian Duriez. Optimization-based Inverse Model of Soft Robots with Contact Handling. *IEEE Robotics and Automation Letters*, 2(3):1413–1419, 2017.

[7] Cosimo Della Santina, Christian Duriez, and Daniela Rus. Model-based control of soft robots: A survey of the state of the art and open challenges. *IEEE Control Systems Magazine*, 43(3):30–65, 2023.

[8] Roy Featherstone. *Rigid Body Dynamics Algorithms*. Springer, 2014.

[9] Michael W Hannan and Ian D Walker. Kinematics and the Implementation of an Elephant's Trunk Manipulator and other Continuum Style Robots. *Journal of Robotic Systems*, 20(2):45–63, 2003.

[10] Hassan K Khalil. *Nonlinear Control*, volume 406. Pearson New York, 2015.

[11] Cecilia Laschi, Matteo Cianchetti, Barbara Mazzolai, Laura Margheri, Maurizio Follador, and Paolo Dario. Soft robot arm inspired by the octopus. *Advanced robotics*, 26(7):709–727, 2012.

[12] Mariangela Manti, Taimoor Hassan, Giovanni Passetti, Nicolò D'Elia, Cecilia Laschi, and Matteo Cianchetti. A Bioinspired Soft Robotic Gripper for Adaptable and Effective Grasping. *Soft Robotics*, 2(3):107–116, 2015.

[13] Andrew D Marchese, Cagdas D Onal, and Daniela Rus. Autonomous Soft Robotic Fish Capable of Escape Maneuvers Using Fluidic Elastomer Actuators. *Soft robotics*, 1(1):75–87, 2014.

[14] Gianmarco Mengaldo, Federico Renda, Steven L Brunton, Moritz Bächer, Marcello Calisti, Christian Duriez, Gregory S Chirikjian, and Cecilia Laschi. A concise guide to modelling the physics of embodied intelligence in soft robotics. *Nature Reviews Physics*, 4(9):595–610, 2022.

[15] Adam Paszke, Sam Gross, Francisco Massa, Adam Lerer, James Bradbury, Gregory Chanan, Trevor Killeen, Zeming Lin, Natalia Gimelshein, Luca Antiga, Alban Desmaison, Andreas Kopf, Edward Yang, Zachary DeVito, Martin Raison, Alykhan Tejani, Sasank Chilamkurthy, Benoit Steiner, Lu Fang, Junjie Bai, and Soumith Chintala. Pytorch: An imperative style, high-performance deep learning library. In *Advances in Neural Information Processing Systems 32*, pages 8024–8035. Curran Associates, Inc., 2019.

[16] Pietro Pustina, Pablo Borja, Cosimo Della Santina, and Alessandro De Luca. P-sati-d shape regulation of soft robots. *IEEE Robotics and Automation Letters*, 8(1): 1–8, 2022.

[17] Ke Qiu, Jingyu Zhang, Danying Sun, Rong Xiong, Haojian Lu, and Yue Wang. An efficient multi-solution solver for the inverse kinematics of 3-section constant-curvature robots. *arXiv preprint arXiv:2305.01458*, 2023.

[18] Federico Renda, Frédéric Boyer, Jorge Dias, and Lakmal Seneviratne. Discrete cosserat approach for multisection soft manipulator dynamics. *IEEE Transactions on Robotics*, 34(6):1518–1533, 2018.

[19] José Guadalupe Romero, Romeo Ortega, and Ioannis Sarras. A globally exponentially stable tracking controller for mechanical systems using position feedback. *IEEE Transactions on Automatic Control*, 60(3):818–823, 2014.

[20] Chia-Hsien Shih, Noel Naughton, Udit Halder, Heng-Sheng Chang, Seung Hyun Kim, Rhanor Gillette, Prashant G Mehta, and Mattia Gazzola. Hierarchical control and learning of a foraging cyberoctopus. *Advanced Intelligent Systems*, page 2300088, 2023.

[21] Mark W. Spong. An historical perspective on the control of robotic manipulators. *Annual Review of Control, Robotics, and Autonomous Systems*, 5:1–31, 2022.

[22] Robert J. III Webster and Bryan A. Jones. Design and kinematic modeling of constant curvature continuum robots: A review. *The International Journal of Robotics Research*, 29(13):1661–1683, 2010.

[23] Hong Kai Yap, Nazir Kamaldin, Jeong Hoon Lim, Fatima A Nasrallah, James Cho Hong Goh, and Chen-Hua Yeow. A Magnetic Resonance Compatible Soft Wearable Robotic Glove for Hand Rehabilitation and Brain Imaging. *IEEE transactions on neural systems and rehabilitation engineering*, 25(6):782–793, 2016.

[24] Davide Zambrano, Matteo Cianchetti, Cecilia Laschi, Helmut Hauser, Rudolf Fuchslin, and Rolf Pfeifer. The Morphological Computation Principles As A New Paradigm For Robotic Design. Opinions and Outlooks on Morphological Computation. *Opinions and Outlooks on Morphological Computation*, 16(25):214–225, 2014.